Atmos. Chem. Phys. Discuss., 12, 23603–23644, 2012
www.atmos-chem-phys-discuss.net/12/23603/2012/
doi:10.5194/acpd-12-23603-2012

Atmospheric Chemistry and Physics Discussions

Observational constraints on ozone radiative forcing from the Atmospheric Chemistry Climate Model Intercomparison Project (ACCMIP)

K. Bowman[1], D. Shindell[2], H. Worden[3], J. F. Lamarque[3], P. J. Young[4,5], D. Stevenson[7], Z. Qu[18], M. de la Torre[1], D. Bergmann[6], P. Cameron-Smith[6], W. J. Collins[8], R. Doherty[6], S. Dalsøren[9], G. Faluvegi[2], G. Folberth[8], L. W. Horowitz[11], B. Josse[12], Y. H. Lee[2], I. MacKenzie[7], G. Myhre[9], T. Nagashima[13], V. Naik[11], D. Plummer[14], S. Rumbold[8], R. Skeie[9], S. Strode[15], K. Sudo[13], S. Szopa[16], A. Voulgarakis[19], G. Zeng[17], S. Kulawik[1], and J. Worden[1]

[1]Jet Propulsion Laboratory-California Institute of Technology, Pasadena, CA, USA
[2]NASA Goddard Institute for Space Studies and Columbia Earth Institute, New York, NY, USA
[3]National Center for Atmospheric Research,Boulder, Colorado, USA
[4]Cooperative Institute for Research in Environmental Sciences, University of Colorado, Boulder, Colorado, USA
[5]Chemical Sciences Division, NOAA Earth System Research Laboratory, Boulder, Colorado, USA

[6]Lawrence Livermore National Laboratory, Livermore, CA, USA
[7]School of GeoSciences, The University of Edinburgh, Edinburgh, UK
[8]Met Office Hadley Centre, UK
[9]Center for International Climate and Environmental Research, Oslo, Norway
[11]NOAA Geophysical Fluid Dynamics Laboratory, Princeton, NJ, USA
[12]GAME/CNRM, Météo-France, CNRS – Centre National de Recherches Météorologiques, Toulouse, France
[13]Nagoya University, Nagoya, Japan
[14]Environment Canada, Canada
[15]NASA Goddard Space Flight Center and Universities Space Research Association, Columbia, Maryland, USA
[16]Laboratoire des Sciences du Climat et l'Environnement, Gif-sur-Yvette, France
[17]National Institute of Water and Atmospheric Research, Lauder, New Zealand
[18]Raytheon Intelligence & Information Systems, Pasadena, CA, USA
[19]Department of Physics, Imperial College London, London, UK

Received: 31 July 2012 – Accepted: 16 August 2012 – Published: 11 September 2012

Correspondence to: K. Bowman (kevin.bowman@jpl.nasa.gov)

Published by Copernicus Publications on behalf of the European Geosciences Union.

Abstract

We use simultaneous observations of ozone and outgoing longwave radiation (OLR) from the Tropospheric Emission Spectrometer (TES) to evaluate ozone distributions and radiative forcing simulated by a suite of chemistry-climate models that participated in the Atmospheric Chemistry and Climate Model Intercomparison Project (ACCMIP). The ensemble mean of ACCMIP models show a persistent but modest tropospheric ozone low bias (5–20 ppb) in the Southern Hemisphere (SH) and modest high bias (5–10 ppb) in the Northern Hemisphere (NH) relative to TES for 2005–2010. These biases lead to substantial differences in ozone instantaneous radiative forcing between TES and the ACCMIP simulations. Using TES instantaneous radiative kernels (IRK), we show that the ACCMIP ensemble mean has a low bias in the SH tropics of up to 100 m W m^{-2} locally and a global low bias of 35 ± 44 m W m^{-2} relative to TES. Combining ACCMIP preindustrial ozone and the TES present-day ozone, we calculate an observationally constrained estimate of tropospheric ozone radiative forcing (RF) of 399 ± 70 m W m^{-2}, which is about 7 % higher than using the ACCMIP models alone but with the same standard deviation (Stevenson et al., 2012). In addition, we explore an alternate approach to constraining radiative forcing estimates by choosing a subset of models that best match TES ozone, which leads to an ozone RF of 369 ± 42 m W m^{-2}. This estimate is closer to the ACCMIP ensemble mean RF but about a 40 % reduction in standard deviation. These results point towards a profitable direction of combining observations and chemistry-climate model simulations to reduce uncertainty in ozone radiative forcing.

1 Introduction

Tropospheric ozone plays a central role in both atmospheric chemistry and climate. Due to significant increases in anthropogenic emissions of its precursors since preindustrial times, tropospheric ozone has the third highest impact as an anthropogenic

ACPD
12, 23603–23644, 2012

greenhouse gas in terms of direct radiative forcing 350 [250–650] m W m^{-2} (Forster et al., 2007) but is distinguished from other greenhouse gases by having significant spatial and temporal heterogeneity due to its relatively short lifetime. Ozone is an essential part of the oxidative capacity of the troposphere, both as an oxidant in its own right, but especially as a precursor of the hydroxyl radical (OH) (Wang and Jacob, 1998; Voulgarakis et al., 2012). Reaction with OH controls the chemical lifetime of many species in the atmosphere, including methane, providing a link between ozone concentrations and the efficacy of methane radiative forcing (Shindell et al., 2005, 2009). Moreover, changes in climate can affect the chemistry of ozone, including increasing (decreasing) the rate of OH production due to higher (lower) water vapor concentrations with warming (cooling) temperatures, with impacts for methane and other gases (e.g. Stevenson et al., 2006). In addition, ozone can indirectly affect the climate through the carbon and hydrological cycles. As it is a phytotoxin, increases in ozone can reduce global primary productivity and therefore the CO_2 uptake by biota (plants, forests), potentially leading to an indirect radiative forcing of a similar magnitude to the direct ozone radiative forcing (Sitch et al., 2007; Collins et al., 2010). Uncertainties in these processes impact knowledge of preindustrial ozone concentrations, the evolution of ozone, and present-day distributions. These factors contribute to the broad range of radiative forcing estimates.

Studies since the Intergovernmental Panel on Climate Change (IPCC) Fourth Assessment Report (AR4) have found that changes in short-lived species, including tropospheric ozone, are expected to have a significant impact on global temperatures, especially over the Northern Hemisphere (H. Levy II et al., 2008; Shindell et al., 2008). In particular, by 2050, Short-Live Climate Forcing (SLCF) agents could be responsible for up to 20 % of simulated global mean annually averaged warming and up to 40 % of the total projected summertime warming in the central United States from 2050–2100 (H. Levy II et al., 2008). However, the contribution of short-lived species to simulated changes in global-mean surface temperature can have a strong dependence on SLCF spatial variability (Shindell and Faluvegi, 2009). These factors have been the impetus

ACPD
12, 23603–23644, 2012

for policy formulation that mitigates both air quality and global warming, (West et al., 2006, 2007; van Vuuren et al., 2006; Ramanathan and Xu, 2010; Shindell et al., 2012; Wallack and Ramanathan, 2009) with the concomitant need for accurate measurements and model results.

The Atmospheric Chemistry and Climate Model Intercomparison Project was initiated to complement the Climate Model Intercomparison Project, Phase 5 (CMIP5) (Taylor et al., 2011) by focusing on the coupling of chemically active atmospheric constituents with climate both historically and in the future (Lamarque et al., 2012). A suite of state-of-the-art chemistry-climate models were driven by common emissions and comparable boundary conditions over different time periods from preindustrial to present-day. In addition, simulations of future climate were calculated using emissions derived from Representative Concentration Pathway (RCP) scenarios (van Vuuren et al., 2011). This approach will help quantify the role of SLCF in past and future climate response across a range of models, which was difficult to do previously (Shindell, 2009). Consequently, ACCMIP will be a valuable resource for the IPCC AR5.

Furthermore, a constellation of satellites that can observe a number of trace gas constituents are now available with global coverage and data records of sufficient length to be useful for the evaluation of ACCMIP simulations. Expanding from analysis in Aghedo et al. (2011b), we evaluate ACCMIP ozone and radiative forcing simulations using global, simultaneous observations of ozone and outgoing longwave radiation (OLR) in the 9.6 micron band (where ozone is radiatively active) from the Tropospheric Emission Spectrometer, which was launched aboard the NASA Aura spacecraft in 2004 (Beer, 2006), using data collected from 2005–2010. We apply TES Instantaneous Radiative Kernels (IRK) to the differences between TES and ACCMIP ozone in order to relate changes in the vertical structure of ozone to reductions in upward outgoing longwave radiation (OLR) (δOLR) at the top-of-the-atmosphere (TOA). The IRK quantifies the sensitivity of OLR to changes in the vertical distribution of ozone at each satellite observation that accounts for variations in temperature, water vapor, and clouds (Worden

ACPD
12, 23603–23644, 2012

et al., 2011). Consequently, we quantify the spatially-resolved longwave (LW) radiative impact of ACCMIP ozone throughout the troposphere with respect to TES.

We then combine the ACCMIP estimate of preindustrial ozone with TES present-day ozone to calculate an observationally constrained ozone radiative forcing. There are several important steps and assumptions needed. First, ozone radiative forcing (RF) from preindustrial to present-day for all of the ACCMIP models are taken from Stevenson et al. (2012). The ACCMIP ozone RF follows the standard definition used in the IPCC, which includes a stratospheric temperature adjustment (Forster et al., 2007). However, we define the change in instantaneous radiative forcing $i\mathrm{RF}^{c}_{m}$ as the instantaneous reduction of OLR from the ACCMIP models relative to TES, i.e., $-\delta$OLR, at top-of-the-atmosphere (TOA). The change in radiative forcing RF^{c}_{m}, which is defined at the tropopause, is approximated empirically from $i\mathrm{RF}^{c}_{m}$, which is defined at TOA, using analysis from Stevenson et al. (2012) and Shindell et al. (2012). We can subsequently combine the RF^{c}_{m} with the ACCMIP RF to compute an observationally constrained ozone RF. Critical to this approach is the assumption that differences between TES and ACCMIP ozone can be attributed to the changes in ozone from the preindustrial period. This assumption is not strictly valid, so we can consider an alternative strategy that calculates ozone RF from ACCMIP models that are radiatively close to TES ozone. Another important set of assumptions is that the "line-by-line" radiative transfer model (RTM) used by TES and climate RTMs used in ACCMIP calculate the same OLR for a given atmospheric state. We investigate this assumption by comparing instantaneous radiative forcing between GISS and TES using the IRK and the GISS RTM.

2 Tropospheric emission spectrometer

Launched in July 2004, the NASA EOS Aura platform is in a polar, Sun-synchronous orbit with an equator crossing time of 13:40 and 02:29 local mean solar time for ascending and descending orbit paths, respectively. The Tropospheric Emission Spectrometer (TES) is a Fourier Transform Spectrometer (FTS) that measures spectrally-resolved

ACPD
12, 23603–23644, 2012

outgoing longwave radiation of the Earth's surface and atmosphere at frequencies between 650–2250 cm^{-1} with unapodized spectral resolution of 0.06 cm^{-1} (Beer, 2006). This spectral resolution is sufficient to resolve pressure-broadened IR absorption lines in the troposphere and allows TES to estimate simultaneous vertical profiles of ozone, water vapor, carbon monoxide, methane, deuterated water vapor as well as atmospheric temperature. Effective cloud pressure and optical depth, surface temperature and land emissivity are also derived from TES radiance spectra, which allows TES to perform ozone retrievals in all-sky conditions (Eldering et al., 2008). Algorithms for radiometric calibration (Worden et al., 2007) retrieval of atmospheric parameters (Bowman et al., 2006), and error characterization (Worden et al., 2004), along with cloud property retrievals (Kulawik et al., 2006) have been described previously. The TES forward model used for computing spectral radiances and Jacobians (Clough et al., 2006) is based on LBLRTM (line-by-line radiative transfer model), which has been used as the basis for a number of radiative transfer models in climate models (Forster et al., 2011).TES radiances have been compared to other satellite and aircraft data (Shephard et al., 2008). There is no detectable trend in residual spectral radiances (observed minus calculated) from 2005–2009 to within 0.6 K (Connor et al., 2011). Previous validation studies of the TES ozone V002 product indicate ozone profiles are biased high in the troposphere (≈ 15 %) relative to ozonesondes (Nassar et al., 2008) and aircraft data (Richards et al., 2008) while total ozone columns are biased high by about 10 DU relative to OMI measurements (Osterman et al., 2008). The optimal estimation technique used operationally on TES provides formal uncertainties (Bowman et al., 2002). These uncertainty estimates were tested by comparisons with northern latitude ozonesondes reported in Boxe et al. (2010), which showed that formal measurement and species interference errors were consistent with empirical calculations.

We use TES V004 ozone profile product for this study, which has been updated relative to the V002 product. Ozonesonde profile comparisons with the Intercontinental Chemical Transport Experiment Ozonesonde Network Study (IONS), the World Ozone and Ultraviolet Data Center (WOUDC), the Global Monitoring Division of the

ACPD
12, 23603–23644, 2012

Earth System Research Laboratory (GMD-ESRL), and the Southern Hemisphere Additional Ozonesonde archives (SHADOZ) have been performed. Approximately 5000 matches with one or more of these data sources are found using the coincidence criteria of ±3 h and a 300 km radius, spanning a latitude range and time-span from 72.5° S to 80.3° N from 2004 to 2008. Analysis of the comparisons are documented in the TES Validation Report V4 http://eosweb.larc.nasa.gov/PRODOCS/tes/validation/TES_Validation_Report_v40.pdf. In the Northern Hemisphere, TES is biased high by about 10–15 % throughout the free troposphere. In the tropics, the bias in the free troposphere is vertically dependent with about a 10 % high bias at about 800 hPa and decreasing to near zero at 200 hPa. The southern midlatitudes show similar features but are slightly low biased (< 5 %) at 200 hPa. Comparisons with ozonesondes and ACCMIP models in Young et al. (2012) are consistent with this more rigorous analysis.

3 Instantaneous radiative Kernels

Following Worden et al. (2011), the logarithmic instantaneous radiative kernel (LIRK) is defined as the sensitivity of outgoing longwave radiative flux at the top-of-the-atmosphere (TOA) to changes in the vertical distribution of ozone:

$$\frac{\partial F_{\mathrm{OLR}}}{\partial \ln q(z_l)} = \int_{\nu}\int_{0}^{2\pi}\int_{0}^{\frac{\pi}{2}} \frac{\partial L_{\mathrm{OLR}}(\nu,\theta,\phi)}{\partial \ln q(z_l)} \cos\theta \sin\theta \mathrm{d}\theta \mathrm{d}\phi \mathrm{d}\nu \quad (1)$$

where ν is frequency, F_{OLR} is the OLR flux defined on $\nu \in [985, 1080]\,\mathrm{cm}^{-1}$, q is ozone as a function of altitude level l, L_{OLR} is the OLR at zenith angle ϕ and azimuth angle θ. The partial derivatives of radiance L are provided by the TES operational radiative transfer algorithm, (Clough et al., 2006), and are used within the retrieval algorithm to estimate the vertical distributions of trace gases, temperature, water vapor, and clouds (Worden et al., 2004; Bowman et al., 2006). Consequently, changes in other

ACPD
12, 23603–23644, 2012

atmospheric parameters are incorporated into the IRK, e.g., retrieved cloud top height will change the altitudes for which OLR is sensitive to ozone variations. From this definition, increases in ozone lead to a reduction in TOA OLR consistent with the ozone greenhouse gas effect.

Equation (1) is treated as an operator in a first order Taylor series expansion to calculate the change in instantaneous longwave radiative forcing between TES and a model ozone through

$$i\mathrm{RF}^{\mathrm{c},j}_{\mathrm{LW,l}} = H_j(z_\mathrm{l})\left[\ln q^{\mathrm{obs}}_j(z_\mathrm{l}) - \ln q^{\mathrm{m}}_j(z_\mathrm{l})\right] \quad (2)$$

where $q^{\mathrm{obs}}_j(z_\mathrm{l})$ and $q^{\mathrm{m}}_j(z_\mathrm{l})$ are the TES and model ozone, respectively, at the j-th location and the l-th level while

$$H_j(z_\mathrm{l}) = -\frac{\partial F^j_{\mathrm{OLR}}}{\partial \ln q_j(z_\mathrm{l})} \quad (3)$$

is defined as the negative of Eq. (1) so that instantaneous radiative forcing is referenced to a reduction in OLR. The total longwave radiative effect (LWRE) is calculated by integrating Eq. (3) in altitude to the tropopause, which will be defined here as the chemical tropopause $q < 150$ ppb with respect to TES ozone. The LWRE can be thought of as the reduction in OLR to a 100 % change in the tropospheric ozone profile (Worden et al., 2011). Since the LWRE is a fractional change referenced to TES ozone, it can not be used to calculate the change to a complete absence of ozone. The absolute flux in the 9.6 micron band ranges between 10–20 $\mathrm{W\,m^{-2}}$ under clear-sky scenes depending on the latitude.

TES ozone, LIRK, and LWRE averaged for 2005–2009 are shown in Fig. 1. The LWRE was integrated to the tropopause height derived from the Goddard Modeling and Assimilation Office (GMAO) GEOS-5 (Molod et al., 2012). LWRE indicates that changes in tropospheric ozone lead to reductions in the absolute flux of less than 10 %. There is a strong sensitivity of up to 35 $\mathrm{m\,W\,m^{-2}}$ in the mid-troposphere extending as

ACPD
12, 23603–23644, 2012

low as 600 hPa and arcing poleward to 200 hPa at 60° N and 60° S. The sensitivities increase in the upper troposphere and lower stratosphere with sensitivities well above 60 m W m^{-2}. There is a seasonal migration of the LIRK maximum across the equator, which follows the change in the inter-tropical convergence zone (ITCZ) and is driven primarily by the seasonal shift in cloud distributions. The seasonal pattern of ozone in the SH is strongly influenced by the presence of biomass burning and lightning leading to a maximum of 60–70 ppb in September-October-November (SON). The impact of biomass burning and lightning in South America, sub-equatorial Africa, and Indonesia are clearly seen. Near source regions, the LWRE exceeds 1 W m^{-2} during SON. During December-January-February (DJF), ozone from biomass burning in Africa north of the (ITCZ) has similarly high LWRE. In most months, there is a persistently high LWRE (> 1 W m^{-2}) over the Middle East. This is driven in part by relatively clear skies and a strong thermal contrast that amplifies the ozone greenhouse gas effect. However, in the summer months, there is an ozone enhancement in the middle troposphere (400–500 hPa) induced by trapping from Saharan and Arabian anticyclones, which also corresponds to the highest magnitude LIRK values in the middle troposphere (Li et al., 2001; Liu et al., 2009).

4 Methodology

4.1 Radiative forcing

Radiative forcing (RF) is a measure of the energy imbalance of the Earth-atmosphere system and is used as a means of quantifying the potential of external agents to perturb that system. In the context of historic climate change, the perturbation is referenced from preindustrial (1850s) to the present-day (2000s). Generally, RF is the change in net irradiance at some altitude. For the IPCC, RF is specifically defined as the change in net irradiance at the tropopause after stratospheric temperatures have relaxed to radiative equilibrium but with the surface and atmospheric state held fixed (Forster

ACPD
12, 23603–23644, 2012

et al., 2007). Methods of calculating radiative forcing from tropospheric ozone from models using "off-line" techniques, i.e., radiative transfer calculations performed independently of a climate model's internal radiation calculation, follow two steps. The first step is to calculate the change in ozone concentration due to changes in anthropogenic emissions including ozone precursors. This change is calculated by forcing a global chemistry-climate model with pre-industrial (usually taken in the 1850s) and present-day emissions in separate "time-slices", which is an interval of time, e.g., 1850–1860. The second step is to calculate the change in longwave and shortwave radiation due to the change in present-day ozone relative to the pre-industrial era using an "off-line" radiative transfer model (RTM) where stratospheric temperatures are allowed to equilibrate resulting in an adjusted radiative flux (Edwards and Slingo, 1996; Stevenson et al., 2006; Knutti and Hegerl, 2008; Stevenson et al., 2012). Radiative forcing is generally referenced at the tropopause, the definition of which can have a significant impact on the final calculation, e.g. flat tropopause set at 100, 150 or 200 hPa, zonally invariant and linear with latitude tropopause (Hansen et al., 2007; Naik et al., 2005), chemical tropopause using 150 ppbv ozone level (Stevenson et al., 2006), and the WMO thermal tropopause (Aghedo et al., 2011b). Radiative forcing is simply the difference between the radiative flux between these two time periods, which can be expressed as:

$$\mathrm{RF}^{\mathrm{m}} = F(\boldsymbol{q}_{\mathrm{p}}^{\mathrm{m}}) - F(\boldsymbol{q}_{\mathrm{o}}^{\mathrm{m}}) \tag{4}$$

where F is the globally, area-weighted average net irradiance (shortwave (SW) plus longwave (LW)) in $\mathrm{m\,W\,m^{-2}}$ including stratospheric readjustment, $\boldsymbol{q}_{\mathrm{p}}^{\mathrm{m}}$ is the vertical distribution (discretized as a vector) of present-day ozone simulated by model "m", and $\boldsymbol{q}_{\mathrm{o}}^{\mathrm{m}}$ is preindustrial ozone for the same model. Implicit in Eq. (4) is temporal averaging over some time-slice. Positive values of RF^{m} imply a reduction in OLR consistent with the tropospheric ozone greenhouse gas effect.

ACPD
12, 23603–23644, 2012

4.2 Observationally constrained radiative forcing

4.2.1 Framework

While there are few reliable observations of preindustrial ozone, there is now a rich suite of global ozone observations, particularly from satellites. These observations can provide constraints on present-day ozone and consequently information on ozone radiative forcing. A simple method of using these observations is to calculate radiative forcing based upon observed present-day ozone but model simulated preindustrial ozone in the following manner:

$$\mathrm{RF}_{\mathrm{m}}^{\mathrm{obs}} = F(\boldsymbol{q}_{\mathrm{p}}^{\mathrm{obs}}) - F(\boldsymbol{q}_{\mathrm{o}}^{\mathrm{m}}), \tag{5}$$

where $\boldsymbol{q}_{\mathrm{p}}^{\mathrm{obs}}$ is the vertical distribution of observed present-day ozone. We consider $\mathrm{RF}_{\mathrm{m}}^{\mathrm{obs}}$ as the observationally constrained estimate of ozone radiative forcing for model "m". $\mathrm{RF}_{\mathrm{m}}^{\mathrm{obs}}$ can be related to RF^{m} in Eq. (4) through:

$$\mathrm{RF}_{\mathrm{m}}^{\mathrm{obs}} = F(\boldsymbol{q}_{\mathrm{p}}^{\mathrm{obs}}) - F(\boldsymbol{q}_{\mathrm{p}}^{\mathrm{m}}) + F(\boldsymbol{q}_{\mathrm{p}}^{\mathrm{m}}) - F(\boldsymbol{q}_{\mathrm{o}}^{\mathrm{m}}) \tag{6}$$

$$= \mathrm{RF}^{\mathrm{c}}{}_{\mathrm{m}} + \mathrm{RF}^{\mathrm{m}} \tag{7}$$

where

$$\mathrm{RF}^{\mathrm{c}}{}_{\mathrm{m}} = F(\boldsymbol{q}_{\mathrm{p}}^{\mathrm{obs}}) - F(\boldsymbol{q}_{\mathrm{p}}^{\mathrm{m}}) \tag{8}$$

is the change in radiative forcing.

For an ensemble of models, the mean constrained radiative forcing is

$$\mathrm{RF}^{\mathrm{obs}} = F(\boldsymbol{q}_{\mathrm{p}}^{\mathrm{obs}}) - \overline{F(\boldsymbol{q}_{\mathrm{o}})} \tag{9}$$

where $\overline{F(\boldsymbol{q}_{\mathrm{o}})}$ is the ensemble mean for M-models. A key assumption in this approach is that the ensemble mean estimate of preindustrial ozone is unbiased. Any bias in

ACPD
12, 23603–23644, 2012

preindustrial ozone will be misconstrued through Eq. (9) as radiative forcing. Model calculations of radiative forcing are inherently more robust against this assumption. Uncertainties common to both present-day and preindustrial ozone, e.g., ozone production from lightning sources, will cancel out in Eq. (4) to the extent that the bias has a radiatively linear impact. Conversely, if patterns of differences between observations and models can be isolated to a specific source or process, then improving that aspect of the model will lead to an improved estimate of preindustrial ozone. However, uncertainties unique to preindustrial ozone will effect both a model-based or present-day observationally-based radiative forcing estimates.

4.2.2 Application to TES data

TES observations, which directly measure outgoing longwave radiation (OLR) in the 9.6 micron band (where ozone absorbs thermal infrared radiation) and have the spectral resolution to disentangle the geophysical quantities, e.g., temperature and clouds driving OLR variability, have the potential to provide observational constraints on radiative forcing. However, there are a number of steps necessary to incorporate TES into the framework in Sect. 4.2.1. TES directly observes instantaneous OLR at the top-of-the-atmosphere (TOA). From Shindell et al. (2012) and Stevenson et al. (2012), instantaneous TOA longwave (LW) radiation is about 16–24 % higher than stratospherically adjusted tropopause LW radiation. Consequently, TES TOA flux is reduced by 20 % to approximate the tropopause LW radiation after stratospheric temperature adjustment. Furthermore, the shortwave (SW) estimate is model derived in order to obtain irradiance because TES does not directly measure that band. This will result in an inconsistency between the ozone implied by TES for the LW and the ozone for the SW. However, the contribution of the error in the SW component to the total flux should be relatively small (Stevenson et al., 2006). Chemistry-climate models calculate the full global and diurnal cycle of ozone whereas TES has a global repeat cycle of 16 days and can only measure twice a day through its ascending and descending nodes. Aghedo et al. (2011a) showed that TES sampling is sufficient to capture zonal scale

ACPD
12, 23603–23644, 2012

variations in ozone when compared to chemistry-climate model simulations. However, this study did not assess whether TES sampling of clouds is sufficient to capture the global impact of radiative coupling of clouds on the ozone absorption of LW radiation. We do not address this question here.

With these caveats, the radiative forcing change in Eq. (8) can be expressed in terms of Eq. (2) as

$$\mathrm{RF}^{\mathrm{c}}_{\mathrm{m}} = \alpha \sum_{i \in \mathrm{D}} \sum_{l \in \mathrm{L}} w_i H_{i,l} (\ln[\boldsymbol{q}^{\mathrm{obs}}_{\mathrm{p}}]_{i,l} - \ln[\boldsymbol{q}^{\mathrm{m}}_{\mathrm{p}}]_{i,l}) \tag{10}$$

where w_i are area-weights, $\alpha = 0.8$ approximates the stratospheric adjustment, D is the set of all observed locations/times and L is the set of altitude levels whose maximum value is at the tropopause, which we choose to be the chemical tropopause $q < 150$ ppb derived from TES ozone. The SW component does not enter into Eq. (10) because the model SW is not constrained by TES and therefore $\mathrm{RF}^{\mathrm{c}}_{\mathrm{SW,m}} = 0$. For comparisons in Sect. 5, we will also quantify the instantaneous change in radiative forcing, which is related to $\mathrm{RF}^{\mathrm{c}}_{\mathrm{m}}$ through simply

$$i\mathrm{RF}^{\mathrm{c}}{}_{\mathrm{m}} = \frac{1}{\alpha} \mathrm{RF}^{\mathrm{c}}{}_{\mathrm{m}}. \tag{11}$$

This approach assumes that the error in approximating the nonlinear change in radiative forcing with respect to q in Eq. (8) with the first order Taylor series expansion in Eq. (10) is small relative to the change in radiative forcing. An additional assumption is that the differences in the radiative transfer model used for RF^{c} is small relative to the radiative transfer models used for RF^{m}. We will investigate this assumption in Sect. 5.2.

ACPD
12, 23603–23644, 2012

5 Results

5.1 ACCMIP simulations

We use TES observations to evaluate the ozone and ozone radiative forcing in the chemistry-climate models that participated in ACCMIP. A complete description of the chemistry-climate and chemical transport models along with their short hand designation (CESM-CAM-superfast, CICERO-OsloCTM2, CMAM, GEOSCCM, GFDL-AM3, GISS-E2-R, GISS-E2-TOMAS, HadGEM2, LMDzORINCA, MIROC-CHEM, MOCAGE, NCAR-CAM3.5, STOC-HadAM3, UM-CAM) can be found in Lamarque et al. (2012). Each were driven by a common set of emissions (Lamarque et al., 2010). The experimental design was based on decadal "time-slice" experiments driven by decadal mean sea surface temperatures (SST). The historic periods included 1850, 1980, and 2000 along with 2030 and 2100 time slices that follow the representative concentration pathways (RCP) (van Vuuren et al., 2011). As described in Lamarque et al. (2012) the level of complexity in the chemistry schemes varied significantly between the models. The physical climate was based on prescribed SSTs for most models with the notable exception of the GISS model, which is integrated with a fully coupled ocean-atmosphere model (Shindell et al., 2012). Following Young et al. (2012), model simulations for the 2000 decade were averaged and then interpolated to the domain of the gridded TES product archived along with the ACCMIP simulations at the British Atmospheric Data Archive (BADC), which is composed of 64 pressure levels at $2 \times 2.5^{\circ}$ spatial resolution. These decadal mean model simulations are then compared against TES ozone for 2005–2010.

5.2 Comparison between GISS and TES

One of the key assumptions in Sect. 4.2.1 is that changes in instantaneous radiative forcing ($i\mathrm{RF}_{\mathrm{m}}^{\mathrm{c}}$) calculated from the TES IRK or a climate model radiative transfer model (RTM) would be the same given the same ozone differences and atmospheric state.

ACPD
12, 23603–23644, 2012

To test this assumption, we first compared the GISS-E2-R model with TES ozone and then calculated iRF_m^c (Eq. 11) based on Eq. (10) and then compared to the same calculation using the GISS off-line radiative transfer code. The area-weighted zonal distribution of iRF_m^c is shown in Fig. 2 calculated independently from the TES IRK and the GISS RTM. The relative distribution is the same with either the TES IRK or GISS RTM. There is an overestimate of the iRF_m^c from the GISS RTM relative to the TES IRK in the Northern Hemisphere poleward of 20° and an underestimate in the tropics and in the Southern Hemisphere. Quantitatively, there is good agreement between the GISS and TES calculations from −30° S to 30° N with a bias of about 15 m W m^{-2}. There is significant disagreement, however, between the peak magnitude at 60° S and 40° N where the GISS RTM calculation is a factor of 2–3 times larger than with the TES IRK. In absolute terms, the global mean change in radiative forcing is small. Under the assumptions discussed in Sect. 4, GISS under predicts ozone radiative forcing by 19 m W m^{-2} using the GISS off-line RTM whereas using the TES IRK, the underestimate is 6 m W m^{-2}, which is a factor of 3 lower.

The reason for these differences are still not well understood. Forster et al. (2011) showed that a suite of different chemistry-climate radiative transfer models agreed well with line-by-line calculations (Clough and Iacono, 1995) to within 10 % for tropospheric ozone and water vapor under clear-sky scenes. Conversely, the TES radiative transfer code is designed directly from line-by-line radiative transfer codes to accurately calculate longwave radiation at high spectral resolution to less than 0.1 % of radiance errors. Potential differences, however, could arise from the assumed atmospheric state or with the linearity assumption in the LIRK. The effects of clouds, water vapor, temperature and emissivity on outgoing longwave radiation are reflected in the IRK sensitivity as well as in the GISS RTM. If the differences are due to the atmospheric state or the way they radiatively couple with tropospheric ozone, then the larger radiative response in the GISS RTM suggests that GISS estimates a less opaque atmosphere in the 9.6 micron band than TES. The IRK assumes that changes in flux are linear with changes in tropospheric ozone for small perturbations. For larger perturbations, the IRK would

ACPD
12, 23603–23644, 2012

over estimate LW flux because the atmosphere is more opaque and will underestimate negative perturbations because the atmosphere is less opaque. However, this is not the response seen in Fig. 2. Nevertheless, the differences between the GISS and TES calculation of $i\mathrm{RF}^{\mathrm{c}}_{\mathrm{m}}$ is insignificant from a climate response perspective.

A potential test would be to compare OLR computed from a climate model atmospheric state with the OLR directly measured by TES. OLR from the climate model ozone could be calculated with the TES RTM while keeping of parts of the atmospheric state constant. The difference in OLR could then be calculated based on both methods. This would test both the absolute OLR and the change in OLR. That analysis is beyond the scope of this paper but will be pursued in the future.

The instantaneous radiative forcing differences shown in Fig. 2 do not include a stratospheric adjustment. Shindell et al. (2012) showed that including a stratospheric adjustment reduced the global mean radiative forcing difference, $\mathrm{RF}^{\mathrm{c}}_{\mathrm{m}}$, between TES and GISS to 16 m W m^{-2} or about 16 % lower than the instantaneous change in $i\mathrm{RF}^{\mathrm{c}}_{\mathrm{m}}$ of 19 m W m^{-2}.

5.3 Application to ACCMIP models

We first compare the zonal-vertical difference between the ACCMIP models and TES ozone from 2005–2010 as shown in Fig. 3 including the ensemble (ENS) in the bottom right. There is a rich diversity in the zonal ozone distribution. The middle to lower troposphere the agreement is generally within 10–15 ppb. In the Northern Midlatitudes (NMLT), the GISS and MOCAGE were larger than TES estimates by more than 10 ppb. On the other hand, CICERO, HadGEM2, MIROC-CHEM, and CMAM tended to underestimate NMLT ozone relative to TES. In the tropical troposphere, most models tend to underestimate ozone. The upper troposphere and lower stratosphere showed stronger differences. The CMAM and MIROC-CHEM models had significantly higher ozone in both the NMLT and the Southern Midlatitudes (SMLT). Conversely, MOCAGE, HadGEM2, STOC-HadAM3, and UM-CAM estimated lower ozone than TES in both

ACPD
12, 23603–23644, 2012

the NMLT and SMLT. However, the TES observation operator was not applied to these models as in Aghedo et al. (2011b), nor has there been any bias correction applied to the TES data. Based on ozonesonde comparisons discussed in Sect. 2, TES is high biased in the Northern Hemisphere, which suggests that the high bias in GISS relative to TES is exacerbated but the slight low bias in the ensemble distribution is likely insignificant. Upper tropospheric ozone retrievals in the tropics are relatively unbiased in TES or even low biased, which indicates that the ensemble model low bias is robust.

The contribution of vertical differences between TES and ACCMIP ozone $i\mathrm{RF}^{c,j}_{\mathrm{LW,I}}$ to $i\mathrm{RF}^{c}_{m}$ are shown in Fig. 4 discretized at TES pressure levels. The zonal cross-section in this figure can be related to the ACCMIP-TES ozone differences in Fig. 3 through Eq. (2). For example, in Fig. 3 a 10 ppb low bias of GISS-E2-R relative to TES ozone at 300 hPa and 15° S leads to about a 5 m W m^{-2} high bias in $i\mathrm{RF}^{c}_{m}$ as shown in Fig. 4. The strong thermal contrast in the tropics increases their importance relative to the extratropics. Underestimates of tropical ozone are amplified in terms of radiative forcing changes relative to the extratropics. Almost half of the ACCMIP models had $i\mathrm{RF}^{c,j}_{\mathrm{LW,I}}$ that exceeded 10 m W m^{-2} at individual pressure levels /. Radiatively significant differences where not confined to the upper troposphere. In several models, tropical differences in ozone at pressures greater than 600 hPa led to $i\mathrm{RF}^{c}_{m}$ exceeding 10 m W m^{-2}. The variability in OLR is the product of the variability of the ozone profile with the sensitivity of OLR to ozone. Comparing the LIRK distributions in Fig. 1 to the $i\mathrm{RF}^{c}_{m}$ attributed to the ozone vertical structure in Fig. 4 suggest that in the tropics and SH, $i\mathrm{RF}^{c}_{m}$ is dominated by the spatial pattern of OLR sensitivity to ozone rather than the differences in variability between upper and middle tropospheric ozone. In the NH, such as with GISS at 60° N and 600 hPa, there are significant differences in ozone but are not radiatively important.

A complimentary perspective is shown in Fig. 5 that shows the spatially distributed instantaneous radiative forcing difference integrated up to the chemical tropopause of $q < 150$ ppb diagnosed from TES. Most ACCMIP models overestimate OLR and therefore underestimate radiative forcing in the SH tropics leading to a positive $i\mathrm{RF}^{c}_{m}$. The overestimate in the Eastern Tropical Atlantic is a persistent feature in all of the ACCMIP

ACPD
12, 23603–23644, 2012

models and is reflected in the ensemble mean. Ozone distributions in the tropical Atlantic are driven by a number of processes but is dominated by lightning (Jacob et al., 1996; Jenkins and Ryu, 2004; Bowman et al., 2009; Sauvage et al., 2007). A second persistent feature is the underestimate centered over Southern Africa. Southern equatorial Africa is an important source of biomass burning (Edwards et al., 2006; Aghedo et al., 2007). Satellite-based "top-down" estimates indicate the emissions from biomass burning are significantly underestimated (Arellano et al., 2006; Jones et al., 2009). Local sources of pollution and biomass burning have been associated with upward trends in ozone, particularly in the lower troposphere (Clain et al., 2009). However, this region has a complex circulation pattern that includes both anticyclonic transport and recirculation as well as direct eastward/westward transport (Garstang et al., 1996; Sinha et al., 2004). Upwind sources of ozone precursors from biomass burning, pollution, and lightning can be advected across this region and advected out to the remote Pacific (Chatfield and Delany, 1990; Chatfield et al., 2002). Some of the radiatively strongest differences (>200 m W m^{-2}) with TES are throughout the tropical Pacific, which may contribute to the SH underestimate. The ACCMIP ensemble shows a persistent pattern in the tropical Pacific with a local maximum near 75 m W m^{-2}. Comparison of the tropical radiative distribution with the zonal distribution in Fig. 4, points to the combination of lower ozone throughout the troposphere that is amplified by the strong mid-tropospheric radiative sensitivity of the southern branch of the LIRK in Fig. 1. Tropical ozone is sensitive to convective mass flux, height, and it's impact on subsequent subsidence, particularly in the Eastern Pacific (Liu et al., 2010). These factors in conjunction with ozone precursors could help explain these features, though they are more prevalent during El Niño periods (Nassar et al., 2009; Chandra et al., 2009) which are not simulated in ACCMIP well due to decadally averaged SST boundary conditions.

The SH tropical and extratropics dominate radiative differences as shown by the vertically integrated zonal distribution in Fig. 6. The ensemble mean OLR is high by about 100 m W m^{-2} between 10–20° S. The mean is strongly influenced by MOCAGE, CESM-CAM, and NCAR-CAM3.5, which vary from 200–400 m W m^{-2} though the latter

ACPD
12, 23603–23644, 2012

two are driven by similar physical climate models. In the NH extratropics, the ensemble mean is approximately zero with the extrema near 100 m W m^{-2} at 30° N decreasing poleward at a rate between linear and exponential. NH high retrieval biases in the TES data will not strongly effect the ensemble mean because of the lower radiative sensitivity. On the other hand, the SH low bias is robust with respect to the TES retrieval bias.

5.4 Observational constraints on ACCMIP radiative forcing

We can use the instantaneous radiative forcing change, $i\mathrm{RF}^{c}_{m}$, quantified in Sect. 5.3 to calculate an observationally constrained ozone radiative forcing following the approach described in Sect. 4.2.1. In Table 1, we integrate the $i\mathrm{RF}^{c}_{m}$ across the tropics (−15° S–15° N), NH and SH extra-tropics along with the total area-weighted average. As noted in Sect. 5.3, the tropics dominate $i\mathrm{RF}^{c}_{m}$ with the largest discrepancies above 250 m W m^{-2} with 5 of the 15 models above 100 m W m^{-2}. While most of the models underestimated ozone in the tropics, there were 2 models that overestimated $i\mathrm{RF}^{c}_{m}$. Similarly, the SH $i\mathrm{RF}^{c}_{m}$ was largely underestimated by as much as ∼ 170 m W m^{-2}. The NH has a much wider response with about half of the models underestimating $i\mathrm{RF}^{c}_{m}$ with differences as high as ∼ 60 m W m^{-2}. There are 6 models whose total $i\mathrm{RF}^{c}_{m}$ are less than or equal to 10 m W m^{-2} whereas the rest have differences greater than 30 m W m^{-2}. The ensemble mean total $i\mathrm{RF}^{c}_{m}$ of 39 ± 41 m W m^{-2} reflects this variation in the standard deviation.

The $i\mathrm{RF}^{c}_{m}$ at TOA does not reflect changes in stratospheric temperatures, which would reach equilibrium within a few months. Assuming dynamical heating is balanced by radiative heating, we can expect a stratospherically adjusted RF^{c}_{m} to be lower than $i\mathrm{RF}^{c}_{m}$. The impact of this adjustment was calculated in Shindell et al. (2012) and Stevenson et al. (2012) to be between 16 % and 24 % for the GISS off-line RTM and the Edwards-Slingo RTM respectively. We will assume an approximate reduction of 20 % between $i\mathrm{RF}^{c}_{m}$ and RF^{c}_{m}, which is reflected in the last column of Table 1.

ACPD
12, 23603–23644, 2012

We can now estimate the observationally constrained radiative forcing by combining ACCMIP and TES using Eqs. (5) and (9) as shown in Table 2. The ACCMIP radiative forcing estimates, including the SW component, are taken from Stevenson et al. (2012) for the $q < 150$ ppb chemical tropopause definition, which is lower than the chemical tropopause diagnosed from TES. For this tropopause definition, the ACCMIP radiative forcing is $373 \pm 66\,\mathrm{m\,W\,m^{-2}}$. The observationally constrained radiative forcing $399 \pm 70\,\mathrm{m\,W\,m^{-2}}$ is calculated using Eq. (5) and the TES LIRK through Eq. (10) using the TES derived chemical tropopause. The resulting RF is adjusted upward by 7 % relative to the ACCMIP RF. The ratio of the standard deviation to the mean decreased slightly from 18 % to 17 %. Most model estimates are corrected modestly towards higher RF though some changes where as high as 40 %. Only one model's RF were lowered.

It's interesting to note that the two models that had the strongest low bias with respect to TES–CESM-CAM and MOCAGE–had the highest (538) and lowest (309), respectively, ozone radiative forcing. The RF is driven in part by a change of only 4.8 Dobson Units (DU) for MOCAGE and a 10 DU for CESM-CAM from preindustrial to present-day (Stevenson et al., 2012). On the other hand, both had the largest upward correction from TES due primarily to the ozone underestimate in the tropics. This suggests that $\mathrm{RF}_{\mathrm{m}}^{\mathrm{obs}}$ for these two models is driven significantly by their preindustrial ozone distributions. An alternate strategy is to assume that models that are close to TES ozone concentrations will have the least bias in preindustrial ozone. Based upon Table 1, we can estimate RF using only those models that are within $10\,\mathrm{m\,W\,m^{-2}}$ of TES in total $i\mathrm{RF}_{\mathrm{m}}^{\mathrm{c}}$. In this case, $\mathrm{RF}^{\mathrm{obs}}$ is $369 \pm 42\,\mathrm{m\,W\,m^{-2}}$, which is about 10 % lower than the ACCMIP RF estimate and about a 40 % reduction in the standard deviation. Alternatively, if we exclude models that have an $i\mathrm{RF}^{\mathrm{c}}$ greater than $100\,\mathrm{m\,W\,m^{-2}}$ then the updated ensemble $\mathrm{RF}^{\mathrm{obs}}$ is $398 \pm 56\,\mathrm{m\,W\,m^{-2}}$, where the standard deviation is 14 % of the mean or about a 22 % reduction in the standard deviation relative to ACCMIP RF.

ACPD
12, 23603–23644, 2012

6 Conclusions

We have presented here the first direct observational constraint on preindustrial to present-day ozone radiative forcing using a combination of ozone and OLR from TES and radiative forcing estimates from ACCMIP. We estimated an observationally constrained radiative forcing of $399 \pm 70\,\mathrm{m\,W\,m^{-2}}$, which is 7 % higher than the ACCMIP estimate of $373 \pm 66\,\mathrm{m\,W\,m^{-2}}$ from Stevenson et al. (2012). Using an alternate strategy of selecting models that capture well TES ozone, the radiative forcing drops to $369 \pm 42\,\mathrm{m\,W\,m^{-2}}$, which is close to the ACCMIP ensemble mean radiative forcing but with a 40 % less standard deviation.

In order to better understand the radiative forcing estimate, we investigated the spatial patterns driving present-day differences in OLR between ACCMIP and TES. Changes in radiative forcing were driven in the ACCMIP models by variations in the SH Tropics where the ensemble mean instantaneous RF ($i\mathrm{RF}^{c}_{\mathrm{m}}$) reached $100\,\mathrm{m\,W\,m^{-2}}$ in some regions. Persistent patterns of $i\mathrm{RF}^{c}_{\mathrm{m}}$ were centered over the tropical Atlantic and over Southern Africa. While the importance of upper tropospheric ozone to radiative forcing is known (Gauss et al., 2003; Lacis et al., 1990), significant changes to OLR ($> 10\,\mathrm{m\,W\,m^{-2}}$) could be attributed to ACCMIP-TES differences at pressures exceeding 600 hPa. While the modest low bias in RF in the NH can be attributed in part to a TES retrieval high bias, the ACCMIP SH low bias is robust in light of the weaker TES tropical retrieval biases.

The methodology for integrating satellite observations and chemistry-climate models is straightforward but carries important assumptions. In particular, this approach is dependent on an unbiased estimate of preindustrial ozone from the ACCMIP ensemble mean. There is considerable opportunity to develop more sophisticated approaches that differentiate patterns of ozone that can be attributed to historic change versus ozone patterns that are common to both preindustrial and present-day ozone. Weighting these patterns appropriately could reduce the sensitivity of an observationally constrained RF estimate to preindustrial ozone biases. There is considerable interest in

ACPD
12, 23603–23644, 2012

using both data and an ensemble of climate models to understand historic change and probabilistically weight future projections (Collins, 2007; Knutti et al., 2002; Tebaldi and Knutti, 2007). There has been little to no application of these methodologies to chemistry-climate projections or the attribution of historic climate change to chemically active agents (Hegerl et al., 1996; Huber and Knutti, 2012; Santer et al., 2007). The combination of these approaches with a process-based analysis (Eyring et al., 2005; Eyring and et al., 2006; Waugh and Eyring, 2008) can help test radiatively important processes against observations in a manner that can reduce our uncertainty in radiative forcing and increase the reliability of future projections.

Acknowledgements. This research was carried out at the Jet Propulsion Laboratory, California Institute of Technology, under a contract with NASA.

KB acknowledges the support of the NASA Aura ROSES program. He also acknowledges some useful codes from Adetutu Aghedo and Rachel Hodos in the initial processing of TES data to netcdf files.

ACCMIP is organized under the auspices of Atmospheric Chemistry and Climate (AC&C), a project of International Global Atmospheric Chemistry (IGAC) and Stratospheric Processes And their Role in Climate (SPARC) under the International Geosphere-Biosphere Project (IGBP) and World Climate Research Program (WCRP).

The CESM project is supported by the National Science Foundation and the Office of Science (BER) of the US Department of Energy. The National Center for Atmospheric Research is operated by the University Corporation for Atmospheric Research under sponsorship of the National Science Foundation.

GZ acknowledges NIWA HPCF facility and funding from New Zealand Ministry of Science and Innovation.

The work of DB and PC was funded by the US Dept. of Energy (BER), performed under the auspices of LLNL under Contract DE-AC52-07NA27344, and used the supercomputing resources of NERSC under contract No. DE-AC02-05CH11231.

W. J. Collins, G. A. Folberth, F. O'Connor and S. T. Rumbold were supported by the Joint DECC and Defra Integrated Climate Programme (GA01101).

VN and LWH acknowledge efforts of GFDL's Global Atmospheric Model Development Team in the development of the GFDL-AM3 and Modeling Services Group for assistance with data processing.

The GEOSCCM work was supported by the NASA Modeling, Analysis and Prediction program, with computing resources provided by NASA's High-End Computing Program through the NASA Advanced Supercomputing Division.

The MIROC-CHEM calculations were performed on the NIES supercomputer system (NEC SX-8R), and supported by the Environment Research and Technology Development Fund (S-7)of the Ministry of the Environment, Japan.

The STOC-HadAM3 work was supported by cross UK research council grant NE/I008063/1 and used facilities provided by the UK's national high-performance computing service, HECToR, through Computational Modelling Services (CMS), part of the NERC National Centre for Atmospheric Science (NCAS).

The LMDz-OR-INCA simulations were done using computing ressources provided by the CCRT/GENCI computer center of the CEA.

The CICERO-OsloCTM2 simulations were done within the projects SLAC (Short Lived Atmospheric Components) and EarthClim funded by the Norwegian Research Council.

The MOCAGE simulations were supported by Météo-France and CNRS. Supercomputing time was provided by Météo-France/DSI supercomputing center.

D. S. and Y. H. Lee acknowledges support from the NASA MAP and ACMAP programs.

D. P. would like to thank the Canadian Foundation for Climate and Atmospheric Sciences for their long-running support of CMAM development.

References

Aghedo, A. M., Schultz, M. G., and Rast, S.: The influence of African air pollution on regional and global tropospheric ozone, Atmos. Chem. Phys., 7, 1193–1212, doi:10.5194/acp-7-1193-2007, 2007. 23621

Aghedo, A. M., Bowman, K. W., Shindell, D. T., and Faluvegi, G.: The impact of orbital sampling, monthly averaging and vertical resolution on climate chemistry model evaluation with satellite

ACPD

12, 23603–23644, 2012

observations, Atmos. Chem. Phys., 11, 6493–6514, doi:10.5194/acp-11-6493-2011, 2011. 23615

Aghedo, A. M., Bowman, K. W., Worden, H. M., Kulawik, S. S., Shindell, D. T., Lamarque, J. F., Faluvegi, G., Parrington, M., Jones, D. B. A., and Rast, S.: The vertical distribution of ozone instantaneous radiative forcing from satellite and chemistry climate models, J. Geophys. Res., 116, D01305, doi:10.1029/2010JD014243, 2011b. 23607, 23613, 23620

Arellano, A. F., Kasibhatla, P. S., Giglio, L., van der Werf, G. R., Randerson, J. T., and Collatz, G. J.: Time-dependent inversion estimates of global biomass-burning CO emissions using Measurement of Pollution in the Troposphere (MOPITT) measurements, J. Geophys. Res, 111, D09303, doi:10.1029/2005JD006613, 2006. 23621

Beer, R.: TES on the Aura Mission: Scientific Objectives, Measurements, and Analysis Overview, IEEE T. Geosci. Remote Sensing, 44, 1102–1105, 2006. 23607, 23609

Bowman, K., Worden, J., Steck, T., Worden, H., Clough, S., and Rodgers, C.: Capturing time and vertical variability of tropospheric ozone: A study using TES nadir retrievals, J. Geophys. Res., 107, 4723, doi:10.1029/2002JD002150, 2002. 23609

Bowman, K. W., Rodgers, C. D., Kulawik, S. S., Worden, J., Sarkissian, E., Osterman, G., Steck, T., Lou, M., Eldering, A., Shephard, M., Worden, H., Lampel, M., Clough, S., Brown, P., Rinsland, C., Gunson, M., and Beer, R.: Tropospheric Emission Spectrometer: Retrieval Method and Error Analysis, IEEE Tr. Geosci. Remote Sensing, 44, 1297–1307, doi:10.1109/TGRS.2006.871234, 2006. 23609, 23610

Bowman, K. W., Jones, D. B. A., Logan, J. A., Worden, H., Boersma, F., Chang, R., Kulawik, S., Osterman, G., Hamer, P., and Worden, J.: The zonal structure of tropical O_3 and CO as observed by the Tropospheric Emission Spectrometer in November 2004 – Part 2: Impact of surface emissions on O_3 and its precursors, Atmos. Chem. Phys., 9, 3563–3582, doi:10.5194/acp-9-3563-2009, 2009. 23621

Boxe, C. S., Worden, J. R., Bowman, K. W., Kulawik, S. S., Neu, J. L., Ford, W. C., Osterman, G. B., Herman, R. L., Eldering, A., Tarasick, D. W., Thompson, A. M., Doughty, D. C., Hoffmann, M. R., and Oltmans, S. J.: Validation of northern latitude Tropospheric Emission Spectrometer stare ozone profiles with ARC-IONS sondes during ARCTAS: sensitivity, bias and error analysis, Atmos. Chem. Phys., 10, 9901–9914, doi:10.5194/acp-10-9901-2010, 2010. 23609

Chandra, S., Ziemke, J. R., Duncan, B. N., Diehl, T. L., Livesey, N. J., and Froidevaux, L.: Effects of the 2006 El Niño on tropospheric ozone and carbon monoxide: implications for dynamics

ACPD
12, 23603–23644, 2012

and biomass burning, Atmos. Chem. Phys., 9, 4239–4249, doi:10.5194/acp-9-4239-2009, 2009. 23621

Chatfield, R. B. and Delany, A.: Convection links biomass burning to increased tropical ozone: However, models will tend to overpredict O_3, J. Geophys. Res.-Atmos., 95, 18473–18488, 1990. 23621

Chatfield, R. B., Guo, Z., Sachse, G. W., Blake, D. R., and Blake, N. J.: The subtropical global plume in the Pacific Exploratory Mission-Tropics A (PEM-Tropics A), PEM-Tropics B, and the Global Atmospheric Sampling Program (GASP): How tropical emissions affect the remote Pacific, J. Geophys. Res., 107, 4278, doi:10.1029/2001JD000497, 2002. 23621

Clain, G., Baray, J. L., Delmas, R., Diab, R., Leclair de Bellevue, J., Keckhut, P., Posny, F., Metzger, J. M., and Cammas, J. P.: Tropospheric ozone climatology at two Southern Hemisphere tropical/subtropical sites, (Reunion Island and Irene, South Africa) from ozonesondes, LIDAR, and in situ aircraft measurements, Atmos. Chem. Phys., 9, 1723–1734, doi:10.5194/acp-9-1723-2009, 2009. 23621

Clough, S. and Iacono, M.: Line-by-line Calculation of atmospheric fluxes and cooling rates .2. application to carbon-dioxide, ozone, methane, nitrous-oxide and the halocarbons, J. Geophys. Res.-Atmos., 100, 16519–16535, 1995. 23618

Clough, S., Shepard, M., Worden, J. R., Brown, P. D., Worden, H. M., Lou, M., Rodgers, C., Rinsland, C., Goldman, A., Brown, L., Eldering, A., Kulawik, S. S., Cady-Pereira, K., Osterman, G., and Beer, R.: Forward Model and Jacobians for Tropospheric Emission Spectrometer Retrievals, IEEE T. Geosci. Remote Sensing, 44, 1308–1323, 2006. 23609, 23610

Collins, M.: Ensembles and probabilities: a new era in the prediction of climate change, Philos. T. Roy. Soc. A, 365, 1957–1970, doi:10.1098/rsta.2007.2068, 2007. 23625

Collins, W. J., Sitch, S., and Boucher, O.: How vegetation impacts affect climate metrics for ozone precursors, J. Geophys. Res., 115, D23308, doi:10.1029/2010JD014187, 2010. 23606

Connor, T. C., Shephard, M. W., Payne, V. H., Cady-Pereira, K. E., Kulawik, S. S., Luo, M., Osterman, G., and Lampel, M.: Long-term stability of TES satellite radiance measurements, Atmos. Meas. Tech., 4, 1481–1490, doi:10.5194/amt-4-1481-2011, 2011. 23609

Edwards, D. P., Emmons, L. K., Gille, J. C., Chu, A., Attié, J.-L., Giglio, L., Wood, S. W., Haywood, J., Deeter, M. N., Massie, S. T., Ziskin, D. C., and Drummond, J. R.: Satellite-observed pollution from Southern Hemisphere biomass burning, J. Geophys. Res.-Atmos., 111, D14312, doi:10.1029/2005JD006655, 2006. 23621

ACPD
12, 23603–23644, 2012

Edwards, J. M. and Slingo, A.: Studies with a flexible new radiation code. I: Choosing a configuration for a large-scale model, Q. J. Roy. Meteorol. Soc., 122, 689–719, doi:10.1002/qj.49712253107, 1996. 23613

Eldering, A., Kulawik, S. S., Worden, J., Bowman, K., and Osterman, G.: Implementation of cloud retrievals for TES atmospheric retrievals: 2. Characterization of cloud top pressure and effective optical depth retrievals, J. Geophys. Res., 113, D16S37, doi:10.1029/2007JD008858, 2008. 23609

Eyring, V., Butchart, N., Waugh, D. W., Akiyoshi, H., Austin, J., Bekki, S., Bodeker, G. E., Boville, B. A., Brühl, C., Chipperfield, M. P., Cordero, E., Dameris, M., Deushi, M., Fioletov, V. E., Frith, S. M., Garcia, R. R., Gettelman, A., Giorgetta, M. A., Grewe, V., Jourdain, L., Kinnison, D. E., Mancini, E., Manzini, E., Marchand, M., Marsh, D. R., Nagashima, T., Newman, P. A., Nielsen, J. E., Pawson, S., Pitari, G., Plummer, D. A., Rozanov, E., Schraner, M., Shepherd, T. G., Shibata, K., Stolarski, R. S., Struthers, H., Tian, W., and Yoshiki, M.: Assessment of temperature, trace species, and ozone in chemistry-climate model simulations of the recent past, J. Geophys. Res., 111, D22308, doi:10.1029/2006JD007327, 2006. 23625

Eyring, V., Harris, N., Rex, M., Sheperd, T., Fahey, D., Amanatidis, G., Austin, J., Chipperfield, M., Dameris, M., De, P., Forster, F., Gettelman, A., Graf, H., Nagashima, T., Newman, P., Pawson, S., Prather, M. J., Pyle, J. A., Salawitch, J., Santer, B., and Waugh, D. W.: A Strategy for Process-Oriented Validation of Coupled Chemistry-Climate Models, B. Am. Meteorol. Soc., 86, 1117–1133, doi:10.1175/BAMS-86-8-1117, 2005. 23625

Forster, P., Ramaswamy, V., Artaxo, P., Berntsen, T., Betts, R., Fahey, D., Haywood, J., Lean, J., Lowe, D., Myhre, G., Nganga, J., Prinn, R., Raga, G., Schulz, M., and Dorland, R. V.: Climate Change 2007: The Physical Science Basis. Contribution of Working Group I to the Fourth Assessment Report of the Intergovernmental Panel on Climate Change, chap. Changes in Atmospheric Constituents and in Radiative Forcing, 131–217, Cambridge University Press, 2007. 23606, 23608, 23612

Forster, P. M., Fomichev, V. I., Rozanov, E., Cagnazzo, C., Jonsson, A. I., Langematz, U., Fomin, B., Iacono, M. J., Mayer, B., Mlawer, E., Myhre, G., Portmann, R. W., Akiyoshi, H., Falaleeva, V., Gillett, N., Karpechko, A., Li, J., Lemennais, P., Morgenstern, O., Oberländer, S., Sigmond, M., and Shibata, K.: Evaluation of radiation scheme performance within chemistry climate models, J. Geophys. Res., 116, D10302, doi:10.1029/2010JD015361, 2011. 23609, 23618

ACPD
12, 23603–23644, 2012

Garstang, M., Tyson, P. D., Swap, R., Edwards, M., Kallberg, P., and Lindesay, J. A.: Horizontal and vertical transport of air over southern Africa, J. Geophys. Res.-Atmos., 101, 23721–23736, 1996. 23621

Gauss, M., Myhre, G., Pitari, G., Prather, M. J., Isaksen, I. S. A., Berntsen, T. K., Brasseur, G. P., Dentener, F. J., Derwent, R. G., Hauglustaine, D. A., Horowitz, L. W., Jacob, D. J., Johnson, M., Law, K. S., Mickley, L. J., Muller, J.-F., Plantevin, P.-H., Pyle, J. A., Rogers, H. L., Stevenson, D. S., Sundet, J. K., van Weele, M., and Wild, O.: Radiative forcing in the 21st century due to ozone changes in the troposphere and the lower stratosphere, J. Geophys. Res., 108, 4292, doi:10.1029/2002JD002624, 2003. 23624

H. Levy II, Schwarzkopf, M. D., Horowitz, L., Ramaswamy, V., and Findell, K. L.: Strong sensitivity of late 21st century climate to projected changes in short-lived air pollutants, J. Geophys. Res., 113, D06102, doi:10.1029/2007JD009176, 2008. 23606

Hansen, J., Sato, M., Kharecha, P., Russell, G., Lea, D. W., and Siddal, M.: Climate change and trace gases, Philos. T. Roy. Soc. A, 365, 1925–1954, doi:10.1098/rsta.2007.2052, 2007. 23613

Hegerl, G. C., von Storch, H., Hasselmann, K., Santer, B. D., Cubasch, U., and Jones, P. D.: Detecting Greenhouse-Gas-Induced Climate Change with an Optimal Fingerprint Method, J. Climate, 9, 2281–2306, 1996. 23625

Huber, M. and Knutti, R.: Anthropogenic and natural warming inferred from changes in Earth's energy balance, Nature Geosci, 5, 31–36, doi:10.1038/ngeo1327, 2012. 23625

Jacob, D., Heikes, B. G., Fan, S.-M., Logan, J. A., Mauzerall, D. L., Bradshaw, J. D., Singh, H. B., Gregory, G. L., Talbot, R. W., Blake, D. R., and Sachse, G. W.: Origin of ozone and NOx in the tropical troposphere: A photochemical analysis of aircraft observations over the South Atlantic basin, J. Geophys. Res.-Atmospheres, 101, 24235–24250, doi:10.1029/96JD00336, 1996. 23621

Jenkins, G. S. and Ryu, J.-H.: Linking horizontal and vertical transports of biomass fire emissionsto the tropical Atlantic ozone paradox during the Northern Hemisphere winter season: climatology, Atmos. Chem. Phys., 4, 449–469, doi:10.5194/acp-4-449-2004, 2004. 23621

Jones, D. B. A., Bowman, K. W., Logan, J. A., Heald, C. L., Liu, J., Luo, M., Worden, J., and Drummond, J.: The zonal structure of tropical O_3 and CO as observed by the Tropospheric Emission Spectrometer in November 2004 – Part 1: Inverse modeling of CO emissions, Atmos. Chem. Phys., 9, 3547–3562, doi:10.5194/acp-9-3547-2009, 2009. 23621

ACPD
12, 23603–23644, 2012

Knutti, R. and Hegerl, G. C.: The equilibrium sensitivity of the Earth's temperature to radiation changes, Nature Geosci., 1, 735–743, 2008. 23613

Knutti, R., Stocker, T. F., Joos, F., and Plattner, G.-K.: Constraints on radiative forcing and future climate change from observations and climate model ensembles, Nature, 416, 2002. 23625

Kulawik, S. S., Worden, J., Eldering, A., Bowman, K., Gunson, M., Osterman, G. B., Zhang, L., Clough, S. A., Shephard, M. W., and Beer, R.: Implementation of cloud retrievals for Tropospheric Emission Spectrometer (TES) atmospheric retrievals: part 1. Description and characterization of errors on trace gas retrievals, J. Geophys. Res., 111, D24204, doi:10.1029/2005JD006733, 2006. 23609

Lacis, A., Wuebbles, D. J., and Logan, J. A.: Radiative forcing of climate by changes in the vertical distribution of ozone, J. Geophys. Res., 95, 9971–9981, doi:10.1029/JD095iD07p09971, 1990. 23624

Lamarque, J.-F., Bond, T. C., Eyring, V., Granier, C., Heil, A., Klimont, Z., Lee, D., Liousse, C., Mieville, A., Owen, B., Schultz, M. G., Shindell, D., Smith, S. J., Stehfest, E., Van Aardenne, J., Cooper, O. R., Kainuma, M., Mahowald, N., McConnell, J. R., Naik, V., Riahi, K., and van Vuuren, D. P.: Historical (1850–2000) gridded anthropogenic and biomass burning emissions of reactive gases and aerosols: methodology and application, Atmos. Chem. Phys., 10, 7017–7039, doi:10.5194/acp-10-7017-2010, 2010. 23617

Lamarque, J.-F., Shindell, D. T., Josse, B., Young, P. J., Cionni, I., Eyring, V., Bergmann, D., Cameron-Smith, P., Collins, W. J., Doherty, R., Dalsoren, S., Faluvegi, G., Folberth, G., Ghan, S. J., Horowitz, L. W., Lee, Y. H., MacKenzie, I. A., Nagashima, T., Naik, V., Plummer, D., Righi, M., Rumbold, S., Schulz, M., Skeie, R. B., Stevenson, D. S., Strode, S., Sudo, K., Szopa, S., Voulgarakis, A., and Zeng, G.: The Atmospheric Chemistry and Climate Model Intercomparison Project (ACCMIP): overview and description of models, simulations and climate diagnostics, Geosci. Model Dev. Discuss., 5, 2445–2502, doi:10.5194/gmdd-5-2445-2012, 2012. 23607, 23617

Li, Q., Jacob, D. J., Logan, J. A., Bey, I., Yantosca, R. M., Liu, H., Martin, R. V., Fiore, A. M., Field, B. D., Duncan, B. N., and Thouret, V.: A tropospheric ozone maximum over the Middle East, Geophys. Res. Lett., 28, 3235–3238, doi:10.1029/2001GL013134, 2001. 23612

Junhua Liu, Logan, J. A., Jones, D. B. A., Livesey, N. J., Megretskaia, I., Carouge, C., and Nedelec, P.: Analysis of CO in the tropical troposphere using Aura satellite data and the GEOS-Chem model: insights into transport characteristics of the GEOS meteorological products, Atmos. Chem. Phys., 10, 12207–12232, doi:10.5194/acp-10-12207-2010, 2010. 23621

ACPD

12, 23603–23644, 2012

Liu, J. J., Jones, D. B. A., Worden, J. R., Noone, D., Parrington, M., and Kar, J.: Analysis of the summertime buildup of tropospheric ozone abundances over the Middle East and North Africa as observed by the Tropospheric Emission Spectrometer instrument, J. Geophys. Res., 114, D05304, doi:10.1029/2008JD010993, 2009. 23612

Molod, A., Takacs, L., Suarez, M., Bacmeister, J., Song, I., and Eichmann, A.: The GEOS-5 Atmospheric General Circulation Model: Mean Climate and Development from MERRA to Fortuna, Tech. Rep. 28, Goddard Space Flight Center, 2012. 23611

Naik, V., Mauzerall, D., Horowitz, L., Schwarzkopf, M. D., Ramaswamy, V., and Oppenheimer, M.: Net radiative forcing due to changes in regional emissions of tropospheric ozone precursors, J. Geophys. Res.-Atmos., 110, D24306, doi:10.1029/2005JD005908, 2005. 23613

Nassar, R., Logan, J., Worden, H., Megretskaia, I. A., Bowman, K., Osterman, G., Thompson, A. M., Tarasick, D. W., Austin, S., Claude, H., Dubey, M. K., Hocking, W. K., Johnson, B. J., Joseph, E., Merrill, J., Morris, G. A., Newchurch, M., Oltmans, S. J., Posny, F., and Schmidlin, F.: Validation of Tropospheric Emission Spectrometer (TES) Nadir Ozone Profiles Using Ozonesonde Measurements, J. Geophys. Res, 113, D15S17, doi:10.1029/2007JD008819, 2008. 23609

Nassar, R., Logan, J. A., Megretskaia, I. A., Murray, L. T., Zhang, L., and Jones, D. B. A.: Analysis of tropical tropospheric ozone, carbon monoxide, and water vapor during the 2006 El Niño using TES observations and the GEOS-Chem model, J. Geophys. Res., 114, D17304, doi:10.1029/2009JD011760, 2009. 23621

Osterman, G., Kulawik, S., Worden, H., Richards, N., Fisher, B., Eldering, A., Shephard, M., Froidevaux, L., Labow, G., Luo, M., Herman, R., and Bowman, K.: Validation of Tropospheric Emission Spectrometer (TES) Measurements of the Total, Stratospheric and Tropospheric Column Abundance of Ozone, J. Geophys. Res., 113, D15S16, doi:10.1029/2007JD008801, 2008. 23609

Ramanathan, V. and Xu, Y.: The Copenhagen Accord for limiting global warming: Criteria, constraints, and available avenues, P. Natl. Acad. Sci., 107, 8055–8062, 2010. 23607

Richards, N. A. D., Osterman, G. B., Browell, E. V., Hair, J. W., Avery, M., and Li, Q.: Validation of Tropospheric Emission Spectrometer ozone profiles with aircraft observations during the Intercontinental Chemical Transport Experiment-B, J. Geophys. Res., 113, D16S29, doi:10.1029/2007JD008815, 2008. 23609

Santer, B. D., Mears, C., Wentzc, F. J., Taylora, K. E., Glecklera, P. J., Wigleyd, T. M. L., Barnette, T. P., Boylea, J. S., andN. P. Gillettg, W. B., Kleina, S. A., Meehld, G. A., Nozawah, T., Piercee,

ACPD
12, 23603–23644, 2012

D. W., Stotti, P. A., Washingtond, W. M., and Wehner, M. F.: Identification of human-induced changes in atmospheric moisture content, P. Natl. Acad. Sci., 104, 15248–15253, 2007. 23625

Sauvage, B., Martin, R. V., van Donkelaar, A., and Ziemke, J. R.: Quantification of the factors controlling tropical tropospheric ozone and the South Atlantic maximum, J. Geophys. Res., 112, D11309, doi:10.1029/2006JD008008, 2007. 23621

Shephard, M. W., Worden, H. M., Cady-Pereira, K. E., Lampel, M., Luo, M., Bowman, K. W., Sarkissian, E., Beer, R., Rider, D. M., Tobin, D. C., Revercomb, H. E., Fisher, B. M., Tremblay, D., Clough, S. A., Osterman, G. B., and Gunson, M.: Tropospheric Emission Spectrometer Spectral Radiance Comparisons, J. Geophys. Res., 113, D15S05, doi:10.1029/2007JD008856, 2008. 23609

Shindell, D.: Atmospheric Chemistry and Climate Model Intercomparison Project (ACC-MIP), IGACtivities Newsletter, 41, 2009. 23607

Shindell, D. and Faluvegi, G.: Climate response to regional radiative forcing during the twentieth century, Nature Geosci., 2, 294–300, doi:10.1038/ngeo473, 2009. 23606

Shindell, D. T., Faluvegi, G., Bell, N., and Schmidt, G. A.: An emissions-based view of climate forcing by methane and tropospheric ozone, Geophys. Res. Lett., 32, L04803, doi:10.1029/2004GL021900, 2005. 23606

Shindell, D. T., Hiram Levy II, Schwarzkopf, M. D., Horowitz, L. W., Lamarque, J.-F., and Faluvegi, G.: Multimodel projections of climate change from short-lived emissions due to human activities, J. Geophys. Res., 113, D11109, doi:10.1029/2007JD009152, 2008. 23606

Shindell, D. T., Faluvegi, G., Koch, D. M., Schmidt, G. A., Unger, N., and Bauer, S. E.: Improved Attribution of Climate Forcing to Emissions, Science, 326, 716–718, 2009. 23606

Shindell, D. T., Pechony, O., Voulgarakis, A., Faluvegi, G., Nazarenko, L., Lamarque, J.-F., Bowman, K., Milly, G., Kovari, B., Reudy, R., and Schmidt, G.: Interactive ozone and methane chemistry in GISS-E2 historical and future climate simulations, Atmos. Chem. Phys. Discuss., submitted, 2012. 23607, 23608, 23615, 23617, 23619, 23622, 23637

Sinha, P., Jaeglé, L., Hobbs, P. V., and Liang, Q.: Transport of biomass burning emissions from southern Africa, J. Geophys. Res., 109, D20204, doi:10.1029/2004JD005044, 2004. 23621

Sitch, S., Cox, P. M., Collins, W. J., and Huntingford, C.: Indirect radiative forcing of climate change through ozone effects on the land-carbon sink, Nature, 448, 791–794, doi:10.1038/nature06059, 2007. 23606

ACPD
12, 23603–23644, 2012

Stevenson, D., Young, P. J., Naik, V., Lamarque, J.-F., Shindell, D. T., Skeie, R., Dalsoren, S., Myhre, G., Berntsen, T., Folberth, G., Rumbold, S., Collins, W. J., MacKenzie, I. A., Doherty, R. M., Zeng, G., van Noije, T., Strunk, A., Bergmann, D., Cameron-Smith, P., Plummer, D., Strode, S. A., Horowitz, L., Lee, Y., Szopa, S., Sudo, K., Nagashima, T., Josse, B., Cionni, I., Righi, M., Eyring, V., Wild, O., and Bowman, K. W.: Tropospheric ozone changes and radiative forcing 1850–2100 in the Atmospheric Chemistry and Climate Model Intercomparison Project (ACCMIP), Atmos. Chem. Phys. Discuss., in preparation, 2012. 23605, 23608, 23613, 23615, 23622, 23623, 23624, 23637, 23638

Stevenson, D. S., Dentener, F. J., Schultz, M. G., Ellingsen, K., van Noije, T. P. C., Wild, O., Zeng, G., Amann, M., Atherton, C. S., Bell, N., Bergmann, D. J., Bey, I., Butler, T., Cofala, J., Collins, W. J., Derwent, R. G., Doherty, R. M., Drevet, J., Eskes, H. J., Fiore, A. M., Gauss, M., Hauglustaine, D. A., Horowitz, L. W., Isaksen, I. S. A., Krol, M. C., Lamarque, J.-F., Lawrence, M. G., Montanaro, V., Müller, J.-F., Pitari, G., Prather, M. J., Pyle, J. A., Rast, S., Rodriguez, J. M., Sanderson, M. G., Savage, N. H., Shindell, D. T., Strahan, S. E., Sudo, K., and Szopa, S.: Multimodel ensemble simulations of present-day and near-future tropospheric ozone, J. Geophys. Res., 111, D08301, doi:10.1029/2005JD006338, 2006. 23606, 23613, 23615

Taylor, K. E., Stouffer, R. J., and Meehl, G. A.: An Overview of CMIP5 and the Experiment Design, B. Am. Meteor. Soc., 93, 485–498, doi:10.1175/BAMS-D-11-00094.1, 2011. 23607

Tebaldi, C. and Knutti, R.: The use of the multi-model ensemble in probabilistic climate projections, Philos. T. Roy. Soc. A, 365, 2053–2075, doi:10.1098/rsta.2007.2076, 2007. 23625

van Vuuren, D., Edmonds, J., Kainuma, M., Riahi, K., Thomson, A., Hibbard, K., Hurtt, G., Kram, T., Krey, V., Lamarque, J.-F., Masui, T., Meinshausen, M., Nakicenovic, N., Smith, S., and Rose, S.: The representative concentration pathways: an overview, Climatic Change, 109, 5–31, doi:10.1007/s10584-011-0148-z, 2011. 23607, 23617

van Vuuren, D. P., Weyant, J., and de la Chesnaye, F.: Multi-gas scenarios to stabilize radiative forcing, Energy Economics, 28, 102–120, 2006. 23607

Voulgarakis, A., Naik, V., Lamarque, J.-F., Shindell, D. T., Young, P. J., Prather, M. J., Wild, O., Field, R. D., Bergmann, D., Cameron-Smith, P., Cionni, I., Collins, W. J., ren, S. B. D., Doherty, R. M., Eyring, V., Folberth, G. A., Horowitz, L. W., Josse, B., McKenzie, I. A., Nagashima, T., Plummer, D. A., Righi, M., Rumbold, S. T., Stevenson, D. S., Strode, S. A., Sudo, K., Szopa, S., and Zeng, G.: Simulations of present-day and future OH and methane lifetime in the ACCMIP project, Atmos. Chem. Phys. Discuss., submitted, 2012. 23606

ACPD
12, 23603–23644, 2012

Wallack, J. S. and Ramanathan, V.: The Other Climate Changers: Why Black Carbon and Ozone Also Matter, Foreign Affairs, available at: http://www.foreignaffairs.com/articles/65238/jessica-seddon-wallack-and-veerabhadran-ramanathan/the-other-climate-changers, 2009. 23607

Wang, Y. H. and Jacob, D. J.: Anthropogenic forcing on tropospheric ozone and OH since preindustrial times, J. Geophys. Res.-Atmos., 103, 31123–31135, 1998. 23606

Waugh, D. W. and Eyring, V.: Quantitative performance metrics for stratospheric-resolving chemistry-climate models, Atmos. Chem. Phys., 8, 5699–5713, doi:10.5194/acp-8-5699-2008, 2008. 23625

West, J. J., Fiore, A. M., Horowitz, L. W., and Mauzerall, D. L.: Global health benefits of mitigating ozone pollution with methane emission controls, P. Natl. Acad. Sci., 103, doi:10.1073/pnas.06002011033, 2006. 23607

West, J. J., Fiore, A. M., Naik, V., Horowitz, L. W., Schwarzkopf, M. D., and Mauzerall, D. L.: Ozone air quality and radiative forcing consequences of changes in ozone precursor emissions, Geophys. Res. Lett., 34, L06806, doi:10.1029/2006GL029173, 2007. 23607

Worden, H. M., Logan, J. A., Worden, J. R., Beer, R., Bowman, K., Clough, S. A., Eldering, A., Fisher, B. M., Gunson, M. R., Herman, R. L., Kulawik, S. S., Lampel, M. C., Luo, M., Megretskaia, I. A., Osterman, G. B., and Shephard, M.: Comparisons of Tropospheric Emission Spectrometer (TES) ozone profiles to ozonesondes: methods and initial results, J. Geophys. Res.-Atmos., 112, D03309, doi:10.1029/2006JD007258, 2007. 23609

Worden, H. M., Bowman, K. W., Kulawik, S. S., and Aghedo, A. M.: Sensitivity of outgoing longwave radiative flux to the global vertical distribution of ozone characterized by instantaneous radiative kernels from Aura-TES, J. Geophys. Res., 116, D14115, doi:10.1029/2010JD015101, 2011. 23607, 23610, 23611

Worden, J., Kulawik, S. S., Shepard, M., Clough, S., Worden, H., Bowman, K., and Goldman, A.: Predicted errors of Tropospheric Emission Spectrometer nadir retrievals from spectral window selection, J. Geophys. Res., 109, D09308, doi:10.1029/2004JD004522, 2004. 23609, 23610

Young, P. J., Archibald, A. T., Bowman, K. W., Lamarque, J.-F., Naik, V., Stevenson, D. S., Tilmes, S., Voulgarakis, A., Wild, O., Bergmann, D., Cameron-Smith, P., Cionni, I., Collins, W. J., Dalsøren, S. B., Doherty, R. M., Eyring, V., Faluvegi, G., Horowitz, L. W., Josse, B., Lee, Y. H., MacKenzie, I. A., Nagashima, T., Plummer, D. A., Righi, M., Rumbold, S. T., Skeie, R. B., Shindell, D. T., Strode, S. A., Sudo, K., Szopa, S., and Zeng, G.: Pre-industrial to end

ACPD
12, 23603–23644, 2012

21st century projections of tropospheric ozone from the Atmospheric Chemistry and Climate Model Intercomparison Project (ACCMIP), Atmos. Chem. Phys. Discuss., 12, 21615–21677, doi:10.5194/acpd-12-21615-2012, 2012. 23610, 23617

ACPD
12, 23603–23644, 2012

Table 1. Change in instantaneous radiative forcing (iRF^c_m) and stratospherically adjusted radiative forcing (RF^c_m) in m W m^{-2}. Stratospheric adjustment is 20 % less that instantaneous RF based upon (Shindell et al., 2012; Stevenson et al., 2012). Tropics are defined from −15° S–15° N.

Model	Tropics iRF^c_m	SH iRF^c_m	NH iRF^c_m	Total iRF^c_m	Total RF^c_m
ENS	79	47	12	39	31
ENS STDev	75	49	32	41	33
CESM-CAM-superfast	256	103	59	115	92
CICERO-OsloCTM2	81	49	42	52	42
CMAM	106	11	23	35	28
GEOSCCM	29	2	−16	0	0
GFDL-AM3	1	−8	−18	−10	−8
GISS-E2-R	67	24	−41	6	5
GISS-E2-R-TOMAS	65	6	−37	0	0
HadGEM2	50	75	33	53	43
LMDzORINCA	−6	13	−6	1	1
MIROC-CHEM	−37	20	16	7	6
MOCAGE	129	169	48	112	90
NCAR-CAM3.5	168	54	26	65	52
STOC-HadAM3	101	85	37	69	55
UM-CAM	96	61	−1	43	34

ACPD
12, 23603–23644, 2012

Table 2. Observational constrained estimate of radiative forcing attributed to present-day ozone change in $\mathrm{m\,W\,m^{-2}}$. $\mathrm{RF^m}$ are from (Stevenson et al., 2012) based on a 150 ppb chemical tropopause derived from each model. The constrained $\mathrm{RF_m^{obs}}$ assumes a 20 % reduction between TOA instantaneous and stratospherically adjusted flux. The ensemble mean (ENS) includes the standard deviation of the $\mathrm{RF_m^{obs}}$.

Model	RF^m	$\mathrm{RF_m^{obs}}$	% change
ENS	373 ±66	399 ±70	7
CESM-CAM-superfast	446	538	20
CICERO-OsloCTM2	401	443	10
CMAM	322	350	9
GEOSCCM	387	387	0
GFDL-AM3	423	415	−2
GISS-E2-R	314	319	2
GISS-E2-R-TOMAS	333	333	0
HadGEM2	303	345	12
LMDzORINCA	351	352	0
MIROC-CHEM	402	407	2
MOCAGE	219	309	41
NCAR-CAM3.5	433	485	12
STOC-HadAM3	437	491	12
UM-CAM	375	410	9

ACPD
12, 23603–23644, 2012

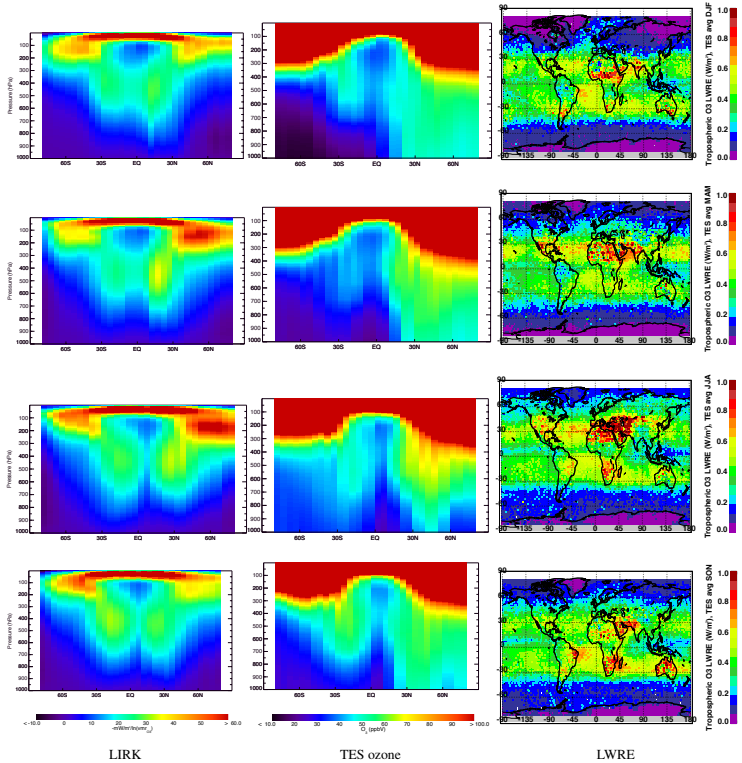

Fig. 1. Logarithmic instantaneous radiative kernels (LIRK) in $-\mathrm{mW\,m^{-2}}/\ln(\mathrm{vmr_{O_3}})$, TES zonal ozone in parts-per-billion (ppb), and Longwave radiative effect (LWRE) in $\mathrm{W\,m^{-2}}$ are shown for each column respectively. Each row represents data averaged for 2005–2009 for December-January-February (DJF), March-April-May (MAM), June-July-August (JJA), and September-October-November (SON).

ACPD
12, 23603–23644, 2012

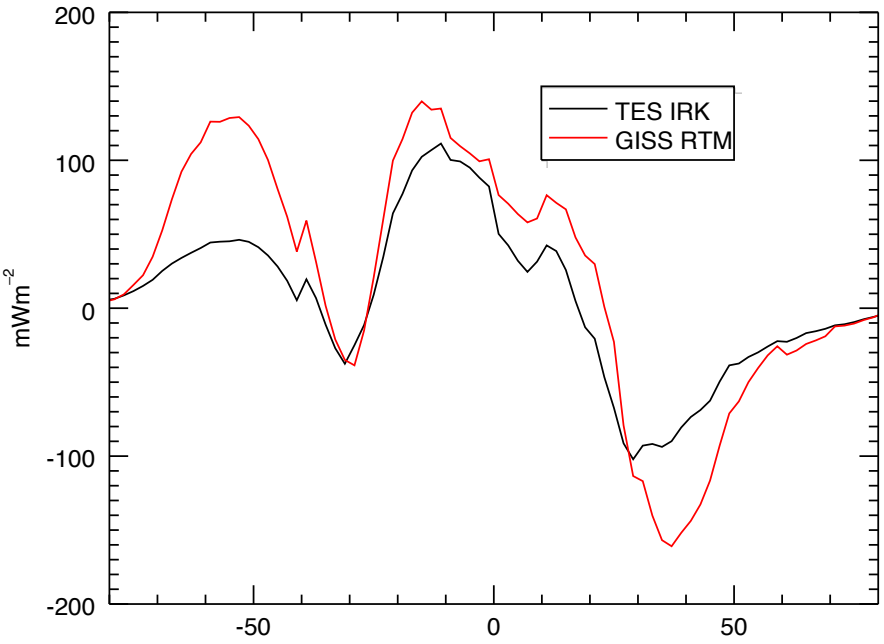

Fig. 2. Comparison of the difference in instantaneous radiative forcing (iRF_m^c) between GISS and TES ozone calculated from the TES IRK and the GISS RTM.

ACPD
12, 23603–23644, 2012

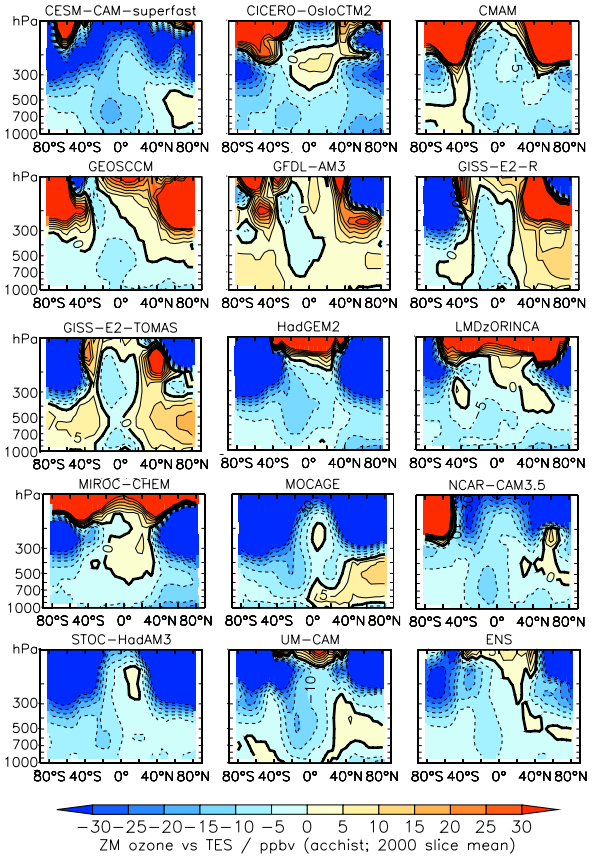

Fig. 3. Zonal difference between ACCMIP models and TES ozone averaged over 2005–2010. Ensemble average of ACCMIP compared to TES ozone is shown under ENS in the bottom right.

ACPD
12, 23603–23644, 2012

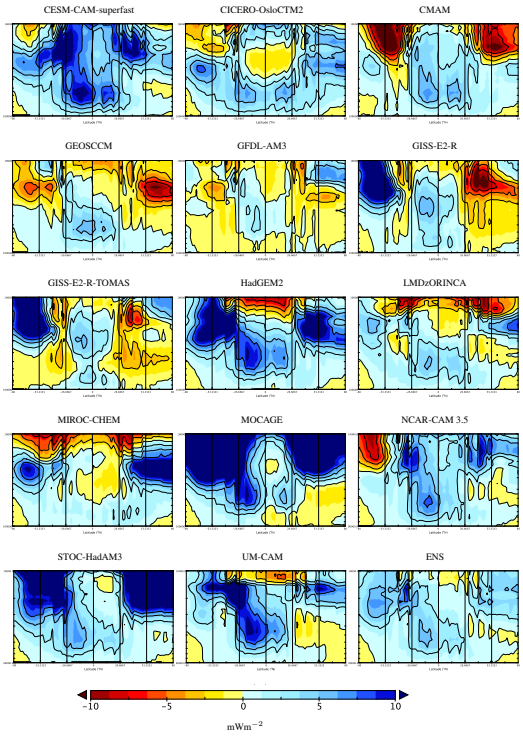

Fig. 4. Zonal distribution of instantaneous radiative forcing, $i\mathrm{RF}^{\mathrm{c}}_{\mathrm{m}}$, attributed to the difference between the ACCMIP and TES ozone profiles from 2005–2010. The vertical scale is defined from 100 000–10 000 Pa discretized to TES pressure levels and the zonal comparison extends from 80° S–80° N with submarkers at 26.6, 53.3° about the equator. Positive values indicate a low bias of $i\mathrm{RF}^{\mathrm{c}}_{\mathrm{m}}$ with respect to TES. Color scale is inverted to show that a low bias in $i\mathrm{RF}^{\mathrm{c}}_{\mathrm{m}}$ is a model underestimate of radiative forcing relative to TES. Ensemble mean bias in $i\mathrm{RF}^{\mathrm{c}}_{\mathrm{m}}$ with respect to TES is denoted by ENS.

ACPD
12, 23603–23644, 2012

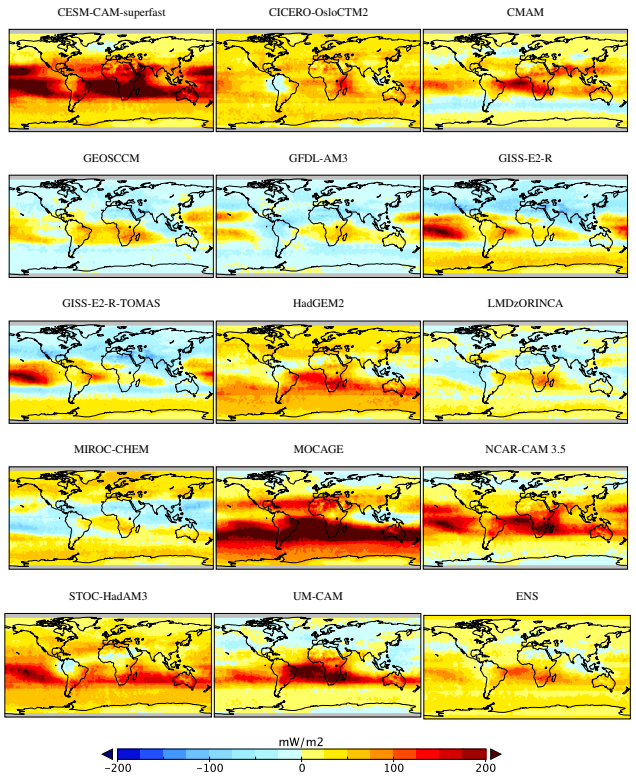

Fig. 5. Spatial distribution of $i\mathrm{RF}_{\mathrm{m}}^{\mathrm{c}}$ between TES and ACCMIP averaged from 2005–2010 and limited to 80° S–80° N. The spatially-resolved instantaneous radiative forcing difference is based on a chemical tropopause $q < 150$ ppb as diagnosed from TES. ACCMIP ensemble is denoted by ENS. Positive values indicate that TES ozone radiative forcing is high relative to the model.

ACPD
12, 23603–23644, 2012

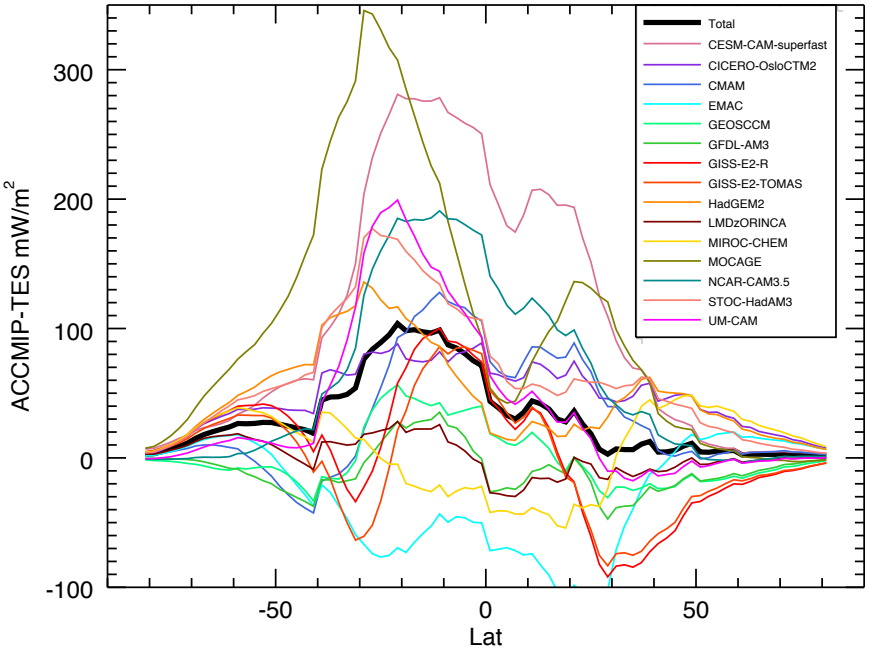

Fig. 6. Zonally distributed iRF_m^c between TES and ACCMIP from 2005–2010 and limited to 80° S–80° N. The instantaneous radiative forcing is based on a TES diagnosed chemical tropopause ($q < 150$ ppb). The Total refers to the ACCMIP ensemble average. Positive values indicate that TES ozone radiative forcing is high relative to the model.

ACPD
12, 23603–23644, 2012